NEOPLASIA
www.neoplasia.com

Volume 18 Number 10 October 2016 pp. 585–593 585

Collagen fibers mediate MRI-detected water diffusion and anisotropy in breast cancers

Samata Kakkad[*,‡], Jiangyang Zhang[*], Alireza Akhbardeh[*], Desmond Jacob[*], Balaji Krishnamachary[*], Meiyappan Solaiyappan[*], Michael A. Jacobs[*,†], Venu Raman[*,†], Dieter Leibfritz[‡], Kristine Glunde[*,†] and Zaver M. Bhujwalla[*,†]

*JHU ICMIC Program, Division of Cancer Imaging Research, The Russell H. Morgan Department of Radiology and Radiological Science; †Sidney Kimmel Comprehensive Cancer Center, The Johns Hopkins University School of Medicine, Baltimore, MD, USA; ‡Department of Chemistry and Biology, University of Bremen, Bremen, Germany

Abstract

Collagen 1 (Col1) fibers play an important role in tumor interstitial macromolecular transport and cancer cell dissemination. Our goal was to understand the influence of Col1 fibers on water diffusion, and to examine the potential of using noninvasive diffusion tensor imaging (DTI) to indirectly detect Col1 fibers in breast lesions. We previously observed, in human MDA-MB-231 breast cancer xenografts engineered to fluoresce under hypoxia, relatively low amounts of Col1 fibers in fluorescent hypoxic regions. These xenograft tumors together with human breast cancer samples were used here to investigate the relationship between Col1 fibers, water diffusion and anisotropy, and hypoxia. Hypoxic low Col1 fiber containing regions showed decreased apparent diffusion coefficient (ADC) and fractional anisotropy (FA) compared to normoxic high Col1 fiber containing regions. Necrotic high Col1 fiber containing regions showed increased ADC with decreased FA values compared to normoxic viable high Col1 fiber regions that had increased ADC with increased FA values. A good agreement of ADC and FA patterns was observed between *in vivo* and *ex vivo* images. In human breast cancer specimens, ADC and FA decreased in low Col1 containing regions. Our data suggest that a decrease in ADC and FA values observed within a lesion could predict hypoxia, and a pattern of high ADC with low FA values could predict necrosis. Collectively the data identify the role of Col1 fibers in directed water movement and support expanding the evaluation of DTI parameters as surrogates for Col1 fiber patterns associated with specific tumor microenvironments as companion diagnostics and for staging.

Neoplasia (2016) 18, 585–593

Introduction

Collagen 1 (Col1) fibers are a major structural component of the extracellular matrix (ECM) of tumors [1]. Increased mammary Col1 fiber density was shown to cause mammary tumor initiation, progression, and metastasis [2]. Col1 fiber topography including fiber diameter [3], directionality [4] and alignment [5] play an

Abbreviations: 2D, two-dimensional; 3D, three-dimensional; aDW, average diffusion weighted; ADC, apparent diffusion coefficient; Col1, collagen 1; DTI, diffusion tensor imaging; ECM, extracellular matrix; ER, estrogen receptor; FA, fractional anisotropy; FOV, field of view; H&E, hematoxylin and eosin; HER-2, human epidermal growth factor receptor 2; HIF-1, hypoxia inducible factor; HRE, hypoxia response element; IDC, invasive ductal carcinoma; LN, lymph node; MRI, magnetic resonance imaging; PFA, paraformaldehyde; PR, progesterone receptor; RFP, red fluorescence protein; SCID, severe combined immunodeficient; SHG, second harmonic generation; VEGF-A, vascular endothelial growth factor A

Address all correspondence to: Zaver M. Bhujwalla, Ph.D., Russell H. Morgan Department of Radiology and Radiological Science, Johns Hopkins University School of Medicine, 208C Traylor Bldg, 720 Rutland Ave, Baltimore, MD 21205.
E-mail: zaver@mri.jhu.edu

Received 26 May 2016; Revised 15 August 2016; Accepted 19 August 2016

1476-5586
http://dx.doi.org/10.1016/j.neo.2016.08.004

important role in cancer motility and invasiveness. Cancer cells can travel along aligned Col1 fibers [6,7]. Tumor associated Col1 fiber alignment is a potential prognostic signature for survival in breast cancer patients [8]. Col1 fibers can be detected with second harmonic generation (SHG) microscopy [1] that detects an intrinsic signal derived from the noncentrosymmetric molecular structure of Col1 fibers [1,9]. Because of limited depth penetration, unless the tissue is superficial, exposed for *in vivo* imaging, or biopsied for *ex vivo* imaging, SHG microscopy cannot be used as a noninvasive imaging modality.

In the brain, water molecules predominantly diffuse along neuronal fibers as diffusion across fibers is restricted by axonal membranes and, in the case of myelinated axons, myelin sheaths. As a result diffusion imaging parameters, *e.g.* apparent diffusion coefficient (ADC) and fractional anisotropy (FA), have been used to visualize fiber tracts and quantitatively measure white matter integrity noninvasively [10–13]. Col1 fibers in the tumor ECM may mediate, in a similar fashion, water diffusion. Diffusion tensor imaging (DTI) detected Col1 architecture, as validated by SHG microscopy, in the carotid artery [14], identifying the potential use of DTI as a noninvasive imaging technique to detect Col1 fibers [14]. Here we investigated the association between diffusion MRI parameters and breast cancer Col1 fiber distribution, to determine if diffusion MRI can provide noninvasive imaging indices of Col1 fibers to use as surrogate markers of aggressiveness.

We determined the correlation between Col1 fibers and water diffusion in MDA-MB-231 human breast cancer xenografts engineered to express red fluorescent protein (RFP) under hypoxia [15], since we previously observed that hypoxic regions contained significantly fewer Col1 fibers [15]. This provided a useful model to easily identify low Col1 fiber regions to relate to the two DTI parameters, apparent diffusion coefficient (ADC) and fractional anisotropy (FA). Additional *ex vivo* studies were performed with human specimens to confirm the observations made with xenografts. Our data identified a close association between Col1 fiber density and DTI parameters in the *in vivo* and *ex vivo* studies supporting further evaluation of ADC and FA as noninvasive indices of Col1 fibers in tumors, and highlighting the importance of Col1 fibers in molecular transport through the ECM.

Methods

Breast Cancer Xenografts

Orthotopically implanted MDA-MB-231 tumors derived from cells containing the hypoxia response element (HRE) of the human vascular endothelial growth factor A (VEGF-A) gene ligated to the cDNA of tdTomato RFP (MDA-MB-231-HRE-TdTomato) were used to identify hypoxia [15,16]. *In vivo–ex vivo* DTI studies were performed on six tumors with an additional five used for *ex vivo* studies alone. An overview of the experimental design is presented as a schematic in Figure 1.

Clinical Specimens

Studies with clinical specimens were performed to determine if the observations made with xenografts were replicated in human specimens. DTI and SHG microscopy were performed on one stage IIB and two stage IIIA invasive ductal carcinoma (IDC) with an approximate size of 10 × 15 mm^2, obtained from Integrated Laboratory Services–Biotech (Chestertown, MD, USA). All tumors were grade 3, estrogen receptor positive (ER+), progesterone receptor

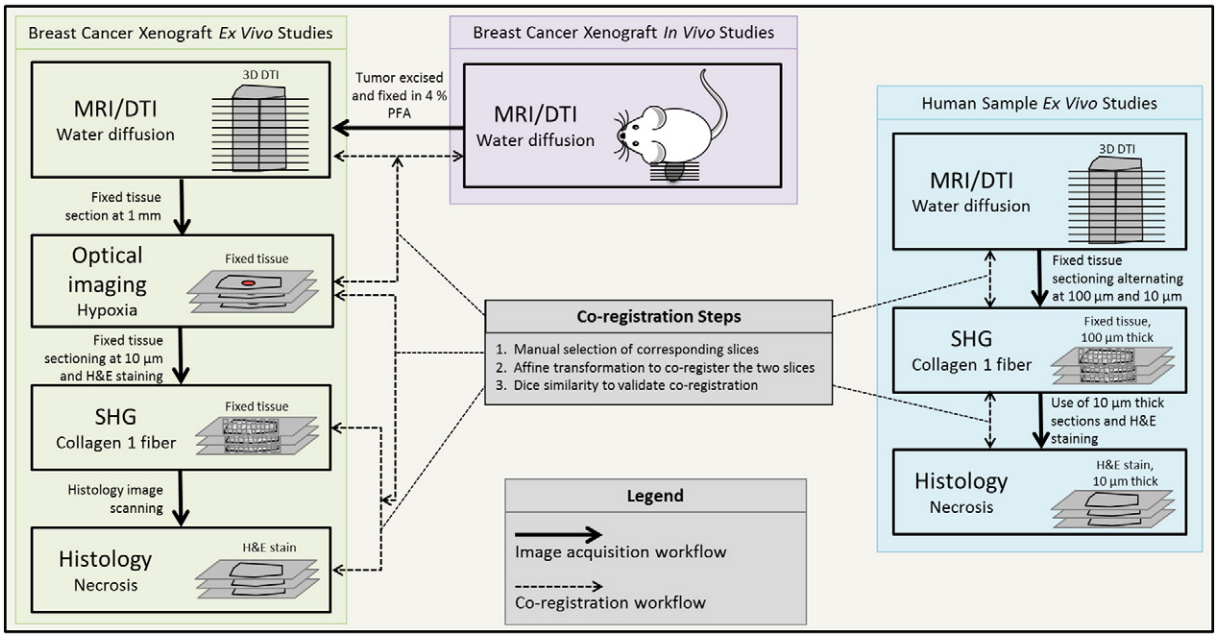

Figure 1. Schematic outline of the workflow. The green box summarizes the *ex vivo* study workflow of breast cancer xenografts. The purple block summarizes the *in vivo* study workflow of breast cancer xenografts. DTI acquisitions were done *in vivo*. Excised tumors were put through the experimental and analytical steps as described in the workflow. Co-registered *in vivo* and *ex vivo* images were used to calculate the correlation between *in vivo* and *ex vivo* measurements for ADC and FA values in hypoxic, normoxic and necrotic regions. The blue box summarizes *ex vivo* study workflow of human breast cancer specimens. Thick arrows indicate the image acquisition workflow, while dashed arrows represent the quantification and analysis workflow.

positive (PR+), Her2 positive (HER2+), and lymph node positive (LN+).

In Vivo DTI Acquisition

In vivo DTI was performed on a horizontal 11.7 T Bruker system (Bruker Corp., Billerica, MA, USA) with a 70 mm inner diameter volume transmit coil and a 10 mm diameter receive-only planar surface coil. Mice were anesthetized with isoflurane and positioned in an animal holder (Bruker BioSpin, Billerica, MA, USA). Respiration was monitored using a pressure sensor (SAII, Stony Brook, NY, USA), and maintained at 40–60 breaths per minute. High-resolution T2-weighted anatomical images of the tumor were acquired using a RARE sequence with imaging parameters of TE/TR = 12.31/3000 ms, 8 averages, FOV = 14 × 10 mm^2, and a matrix of 192 by 144 with 20 z-slices of 0.4 mm thickness. For the same FOV, diffusion-weighted images were acquired using a modified EPI sequence with imaging parameters of TE/TR = 23.6/5000 ms, two repetitions, five non–diffusion-weighted and 30 diffusion directions, b-value ~1500 s/mm^2, FOV = 14 × 10 mm^2, matrix size of 128 × 96, native imaging resolution =105 × 105 μm^2, and 20 z-slices. The *in vivo* data were acquired at a lower resolution that permitted the 30 direction data to be acquired within an acceptable overall imaging time of less than 1 hour.

Ex Vivo DTI Acquisition

Samples fixed for 24 hours in 4% paraformaldehyde (PFA), were washed with phosphate buffered saline for 72 hours, and placed in a 10 mm NMR tube immersed in Fomblin perfluoro polyether solution (Solvay Sollexis). MRI was performed on a vertical 11.7 T Bruker Avance NMR spectrometer (Bruker Biospin, Billerica, MA, USA) equipped with micro-imaging accessories. A Micro 2.5 gradient set capable of maximum 1500 mT/m gradient strength with a 10 mm birdcage volume coil was used. High-resolution T2-weighted MRI, and DTI of the samples were performed in 3D with an isotropic resolution of 62.5 × 62.5 × 62.5 μm^3. DTI was performed using a modified 3D diffusion-weighted gradient and spin echo (DW-GRASE) sequence [17] with the following parameters: TE/TR = 36/1500 ms, 4 signal averages, two non–diffusion-weighted images and six diffusion directions, b = 2100 s/mm^2, field of view (FOV) = 8 × 8 × 9 mm^3, a matrix size of 128 × 128 × 150. For the *ex vivo* studies, DT images were acquired at high resolution to compare the DTI data to the high resolution microscopy and histopathology datasets. These high resolution scans took ~15 hours, and therefore had to be limited to six diffusion directions.

Average diffusion-weighted (aDW) images and maps of ADC and FA were calculated using DTI Studio image processing software [18] for both *in vivo* and *ex vivo* DTI data. Both *in vivo* and *ex vivo* experiments were performed at 37°C. The specimen temperature was maintained by an integrated temperature control system that monitored and maintained the bore temperature with warm air.

SHG and Confocal Microscopy

Excised tumors were sectioned at 1 mm slice thickness using a tissue slicer (Braintree Scientific, Inc., Braintree, MA). Hypoxic regions were visualized by fluorescence microscopy using a 1× objective attached to a Nikon microscope, equipped with a Nikon Coolpix digital camera (Nikon Instruments, Inc., Melville, NY). Bright field images were acquired to assess tissue architecture. Following optical imaging, tumors were paraffin-embedded and sectioned at 5 μm thickness for immunohistochemistry and H&E staining. Tile scan SHG microscopy of the entire slice was performed on the first H&E section from each 1 mm slice to acquire Col1 fiber maps in 3D using an Olympus Laser Scanning FV1000 MPE multiphoton microscope (Olympus Corp., US headquarters–Center Valley, PA), with an incident laser wavelength of 860 nm and detection wavelength of 430 nm. A 25× lens was used to acquire confocal z-stacks with tile scan acquisition performed in x and y directions to cover the entire tissue section with FOV 390 × 390 μm^2, and z-intervals of approximately 3 μm.

In human breast cancer samples, Col1 fibers from the entire tumor slice were obtained with SHG microscopy using a Zeiss 710 NLO Meta confocal microscope (Carl Zeiss Micro-Imaging, Inc.), as previously described [15,19,20]. Col1 fibers were acquired using a 25× lens, with excitation wavelength of 880 nm and detection wavelength window of 420–460 nm. Tile scan acquisition was performed in x and y directions with FOV of 339.84 × 339.84 μm^2, with confocal z-stacks approximately 3 μm on the central section of the tumor.

Col1 fiber volume and density quantification was done in MATLAB (Mathworks Inc.) as previously described [15]. Normal breast tissue and tissue adjacent to cancer have been identified to contain wavy fiber patterns [21], whereas aligned-straight fibers were identified in aggressive human breast cancer [7,8,19]. We therefore performed texture analysis of the Col1 fibers to quantify the amounts of straight, mixed and wavy patterns distributed in the clinical specimens and relate these to the DTI parameters. To quantify the Col1 fiber distribution in clinical specimens, the fiber textural patterns were characterized using texture analysis [22] to extract Haralick texture features [23]. By using fuzzy C-mean clustering [24] (5–7 clusters), Haralick texture features were clustered and color-coded in 3D projected SHG images to represent the 3D fiber information within a tumor section in 2D, to differentiate straight, mixed and wavy Col1 fiber patterns.

Co-Registration Strategy for Ex Vivo and In Vivo Co-Localization Quantification

To co-localize maps of Col1 fiber, hypoxia, and water diffusion, affine transformation based co-registration was performed as previously described [20,25] (Figure 1). Briefly, xenograft *in vivo* and *ex vivo* DTI datasets were first co-registered, following which the hypoxia optical images were co-registered to the DTI datasets. The H&E and SHG datasets were first co-registered with each other and then to the hypoxia optical images. In human specimens, the central SHG images were co-registered to the corresponding central *ex vivo* DT images for co-localization and quantification. For both studies, H&E sections were co-registered to corresponding SHG images to detect necrotic regions. We used a linear method of co-registration between the datasets and used the Dice similarity index [26] to evaluate the accuracy of co-registration. A Dice similarity index >0.85 was considered as successful co-registration.

In xenografts, hypoxic regions were identified from co-registered optical fluorescence images, and necrotic regions were identified from co-registered H&E images. *In vivo* and *ex vivo* ADC and FA values were calculated in normoxic, hypoxic and necrotic regions and compared for all mice (*in vivo* N = 6, *ex vivo* N = 11). Percent fiber volume and inter-fiber distances were also calculated for normoxic, hypoxic and necrotic regions.

In human cancers, the SHG Col1 fiber distribution image was used to predict the water diffusion image using a previously described

technique [11]. The predicted diffusion and water diffusion direction maps were compared to the DTI acquired ADC, FA, and color-coded water direction maps [11]. ADC and FA values were calculated in masks of four segmented categories in the SHG images for density and sparseness and masks of three segmented categories for textural patterns. Fiber density and sparseness were segmented into masks of dense (75% < percent fiber volume, inter-fiber distance <1 μm), intermediate-1 (50% < percent fiber volume < 75%, 2 μm < inter-fiber distance <5 μm), intermediate-2 (25% < percent fiber volume < 50%, 2 μm < inter-fiber distance <5 μm) and sparse (percent fiber volume < 25%, 5 μm < inter-fiber distance) fibers. Three textural masks were segmented by fuzzy c-mean clustering [24,27] from the combined Haralick texture feature maps into straight, mixed, and wavy patterns of fiber distribution. The ADC and FA values were calculated in random 10 equidistantly spaced regions of interests (ROIs) for each mask from the central section of each tumor for both quantifications.

Because of the limited samples, a paired one-tailed *t* test ($\alpha = 0.05$) was used to detect significant differences between different categories for both studies using Microsoft Office Excel 2007 (Microsoft, Redmond, WA). A one-tailed *t* test was used since our hypothesis that ADC and FA values would increase in regions with higher percent fiber volume was based on previous studies [11,12,18,20]. $P < .05$ were considered significant.

Fibroblast Immunostaining

Immunohistochemistry was performed to detect activated smooth muscle actin (α-SMA) that is expressed by activated fibroblasts, to determine if infiltration of activated fibroblasts could explain the presence of higher Col1 fibers in necrotic regions. α-SMA immunohistochemistry of an adjacent tumor section to the H&E section was performed using the streptavidin–peroxidase technique and the DAKO EnVision System (Dako Cytomation, Hamburg, Germany) as previously described [28] using the alkaline conjugated monoclonal anti-α-SMA antibody (clone 1 A4) primary antibody (Sigma; 1:200 dilution, 4 °C overnight). High-resolution digital scans of the immunostained sections were obtained using ScanScope (Aperio).

Results

Breast Cancer Xenograft In Vivo–Ex Vivo Studies

Representative images comparing *in vivo* and *ex vivo* DTI data from the same tumor are shown in Figure 2. Good spatial co-localization of ADC and FA features between *in vivo* and *ex vivo* images is evident from these representative images (Figure 2, *A–F*).

Comparisons of *in vivo* and *ex vivo* ADC maps are shown in Figure 2, *A* and *D*, FA maps in Figure 2, *B* and *E*, and water diffusion directionality in Figure 2, *C* and *F*. The corresponding optical red fluorescence image, the H&E stained histological section, and Col1 fiber image are displayed in Figure 2, *G–I*. Overlay images of hypoxia (red) with *in vivo* ADC and FA maps and *ex vivo* ADC and FA maps are shown in Figure 2, *J–M*. We observed a reduction of Col1 fibers in hypoxic tumor regions as shown in Figure 2*N*.

Quantified data summarized for six *in vivo* and eleven *ex vivo* xenograft tumors are shown in Figure 3. Hypoxic regions had significantly lower percent Col1 fiber volume (25 ± 4%) compared to normoxic regions (28 ± 4%) (Figure 3*A*, *P*-value = 0.039, N = 9). Necrotic regions had significantly higher percent fiber volume (31 ± 3%) compared to normoxic ($P = .043$, N = 9) and hypoxic regions ($P = .018$, N = 9). In the xenografts *in vivo*, low Col1 fiber containing hypoxic areas tended towards lower ADC values as compared to the normoxic regions, but ADC values in the necrotic regions (5.47E-04 ± 2.25E-5 mm^2/s) were significantly higher compared to both normoxic (4.72E-04 ± 1.69E-5 mm^2/s, $P = .002$, N = 6) and hypoxic (4.66E-04 ± 1.41E-5 mm^2/s, $P = .004$, N = 6) tumor regions (Figure 3*B*). Significantly lower ADC values were observed in hypoxic regions as compared to the normoxic regions for *ex vivo* data (Figure 3*C*, $P = .005$, N = 11) and significantly higher ADC values were observed in necrotic regions (7.38E-04 ± 2.41E-05

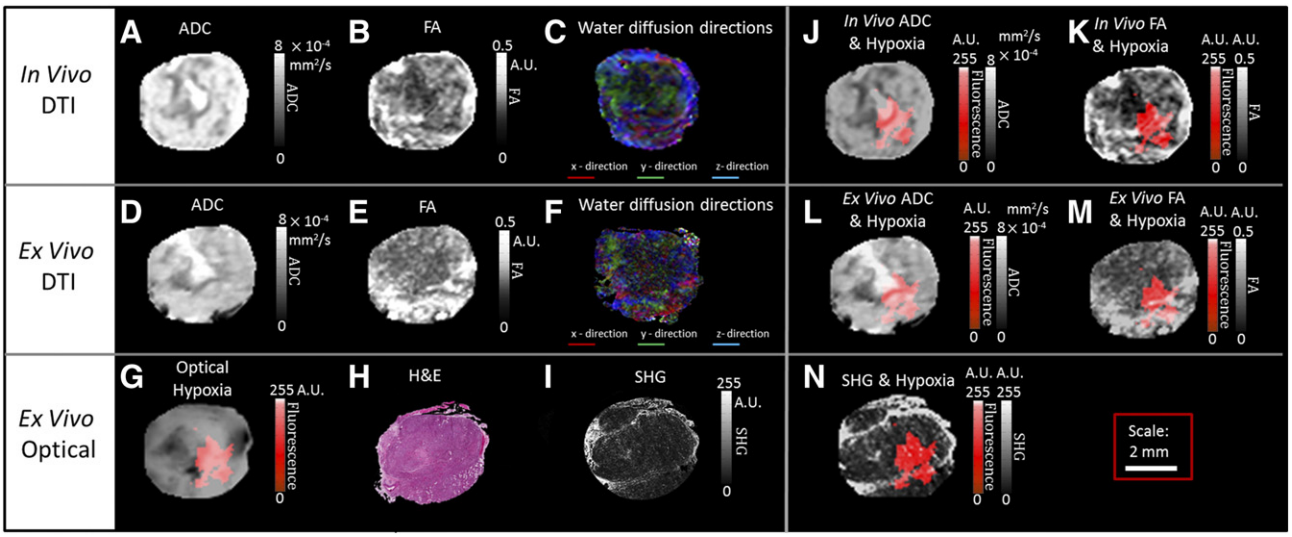

Figure 2. Comparison between *in vivo* and *ex vivo* DTI data in breast cancer xenografts. Representative *in vivo* DT images of (A) ADC map, (B) FA map, and (C) water diffusion directionality color map. Corresponding *ex vivo* DT images of (D) ADC map, (E) FA map, and (F) water diffusion directionality color map. *Ex vivo* optical images of (G) hypoxic fluorescing regions, (H) H&E, and (I) SHG Col1 fibers. Overlay of hypoxic regions (red) with (J) *in vivo* ADC map, (K) *in vivo* FA map, (L) *ex vivo* ADC map, (M) *ex vivo* FA maps and (N) with SHG Col1 fibers. Scale bar of 2 mm for all images (A-N).

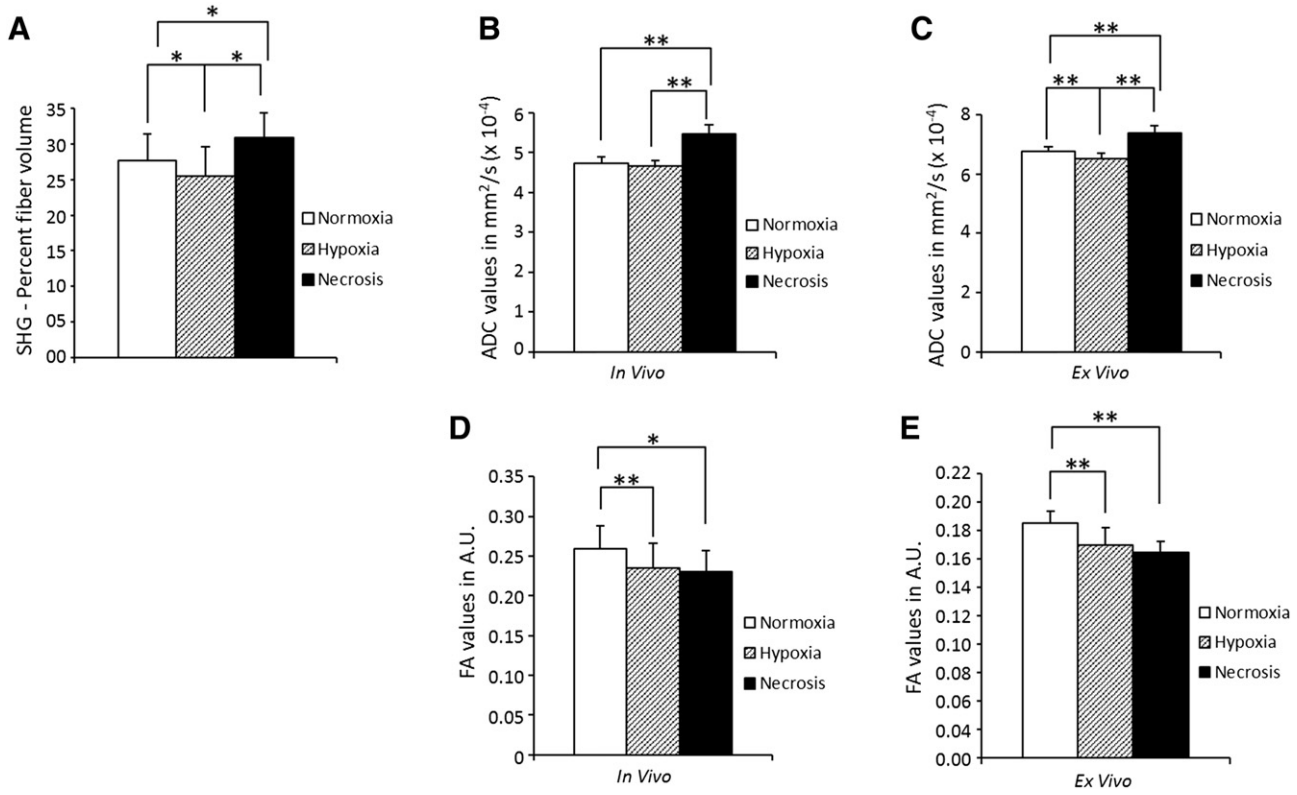

Figure 3. Quantification of *in vivo* and *ex vivo* DTI and SHG data in breast cancer xenografts. (A) Significantly lower percent Col1 fiber volume was observed in hypoxic compared to normoxic ($P = .039$, N = 9) and necrotic regions ($P = .018$, N = 9). Necrotic regions had significantly higher percent fiber volume as compared to normoxic regions ($P = .043$, N = 9). (B) *In vivo*, significantly higher ADC values were observed in necrotic regions compared to normoxic ($P = .002$, N = 6) and hypoxic regions ($P = .004$, N = 6). (C) *Ex vivo*, significantly lower ADC values were observed in hypoxic compared to normoxic ($P = .005$, N = 11), hypoxic compared to necrotic regions ($P = .001$, N = 11), and normoxic compared to necrotic regions ($P = .004$, N = 11). (D) *In vivo*, significantly lower FA values were observed in hypoxic ($P = .016$, N = 6) and necrotic regions ($P = .058$, N = 6), compared to normoxic regions. (E) *Ex vivo*, significantly lower FA values were observed in hypoxic ($P = .011$, N = 11) and necrotic regions ($P = .006$, N = 11), compared to normoxic regions. Values represent Mean ± SEM. $^{**}P \leq .01$, $^{*}P < .05$.

mm^2/s) as compared to the normoxic (6.77E-04 ± 1.57E-05 mm^2/s, $P = .004$, N = 11) and hypoxic (6.51E-04 ± 2.05E-05 mm^2/s, $P = .001$, N = 11) regions. Significantly lower FA values were observed in hypoxic (*in vivo* = 0.24 ± 0.03; *ex vivo* = 0.15 ± 0.01) compared to normoxic regions (*in vivo* = 0.26 ± 0.03; *ex vivo* = 0.17 ± 0.01) for both *in vivo* (Figure 3*D*, $P = .016$, N = 6) and *ex vivo* data (Figure 3*E*, *P*-value = 0.011, N = 11) and significantly lower FA values were observed in necrotic regions (*in vivo* = 0.23 ± 0.03; *ex vivo* = 0.15 ± 0.01) as compared to normoxic regions for both *in vivo* (Figure 3*D*, $P = .058$, N = 6) and *ex vivo* data (Figure 3*E*, $P = 0.006$, N = 11).

Human Sample Ex Vivo Studies

We observed distinct heterogeneities in the diffusion images of human breast cancer samples as shown in Figure 4, similar to the xenograft data. Displayed in Figure 4, *A–D* are representative aDW, ADC, FA, and color-coded water diffusion directionality maps. The corresponding H&E stained histological section is shown in Figure 4*E*. Col1 fiber images displayed similar patterns to the aDW, ADC and FA maps as observed in the corresponding DTI images (Figure 4*F*). We simulated water diffusion anisotropy and directionality maps from the SHG data (Figure 4, *G–H*). The results closely matched the measured FA and water diffusion directionality maps (Figure 4, *C–D*).

To characterize the Col1 fiber patterns, texture analyses of the SHG images were performed and Haralick texture features calculated. Using fuzzy c-mean clustering, Haralick texture features were clustered to color-code 2D projected SHG images with 3D fiber pattern information, to categorize Col1 fiber patterns into straight, mixed and wavy texture patterns (Figure 4*I*). An overlay of the ADC map (gray) with the SHG image (red) is displayed in Figure 4*J*, an overlay of the FA map (gray) with the SHG image (red) is displayed in Figure 4*K*, and an overlay of the FA map (gray) with the simulated diffusion map (red) is displayed in Figure 4*L*. These overlay images identified a close association between Col1 fibers, water diffusion and anisotropy.

Fiber content and fiber distribution was quantified from 10 randomly selected equally spaced ROIs for each tumor (Figure 5). We observed that regions with sparse fibers had reduced ADC values (5.27×10^{-4} mm^2/s) as compared to regions containing intermediate-2 (9.35×10^{-4} mm^2/s), or intermediate-1 (11.03×10^{-4} mm^2/s) fibers. ADC values of sparse fiber regions were significantly lower than ADC values in dense fiber regions (12.00×10^{-4} mm^2/s, $P = .05$, N = 3) (Figure 5*A*). Similar to ADC, FA values were lower in regions with sparse fibers (0.08 ± 0.047) as compared to regions with intermediate-2 (0.17 ± 0.03) or intermediate-1 (0.21 ± 0.03) fibers. FA values in sparse fiber regions were significantly lower than values in regions with dense (0.21 ± 0.01, $P = .057$, N = 3) Col1 fibers (Figure 5*B*). The four fiber content masks of dense fiber regions (red), intermediate-1 fiber regions (gray), intermediate-2 fiber regions

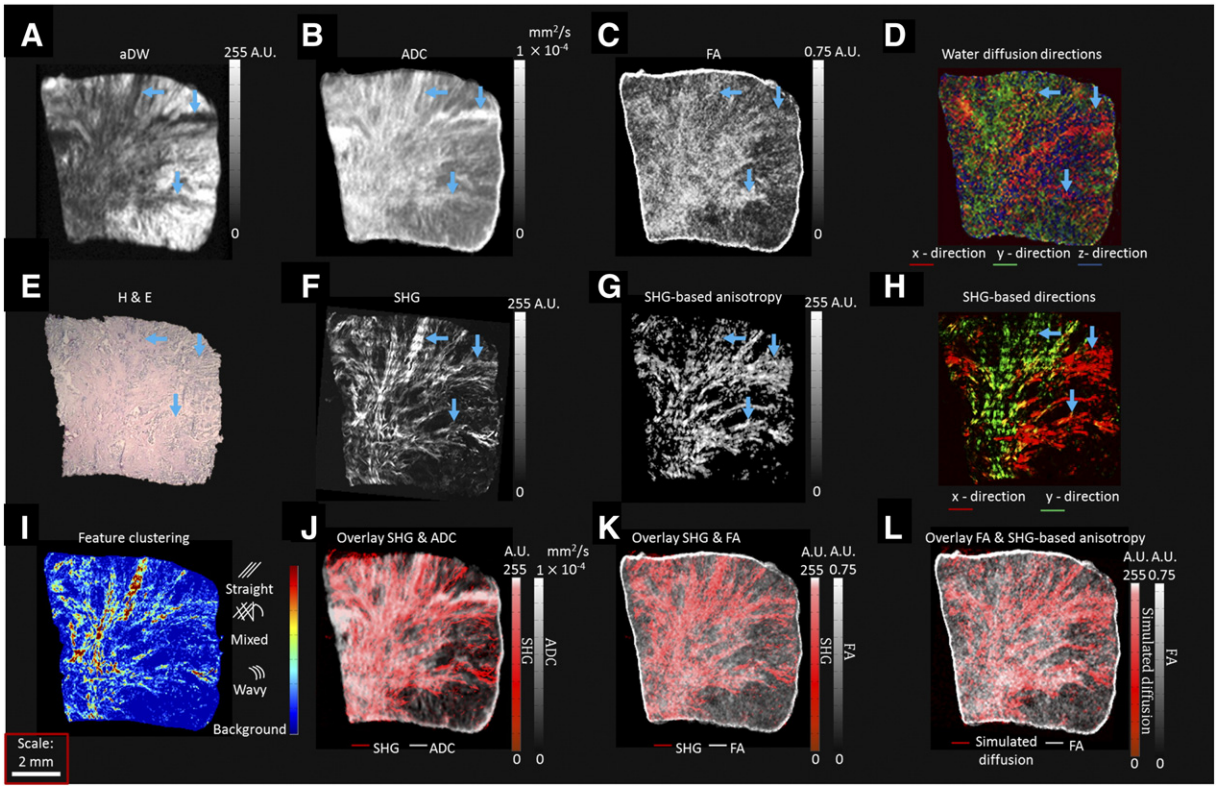

Figure 4. Representative images of a human breast cancer specimen. (A) Representative aDW image, (B) corresponding ADC map, (C) corresponding FA map, (D) corresponding water diffusion direction color map, (E) corresponding H&E section, (F) corresponding SHG map of Col1 fiber distribution. (G) Water diffusion and (H) water diffusion directionality simulated from SHG Col1 fiber images. (I) Color-coded SHG image for straight, mixed and wavy fiber patterns based on texture analysis, (J) overlay of ADC map (gray) and SHG image (red), (K) overlay of FA map (gray) and SHG image (red), and (L) overlay of measured FA map (gray) and simulated diffusion map (red). Scale bar of 2 mm for all images (A-L).

(green), and sparse fiber regions (blue) are shown in Figure 5*C*. From our texture analysis approach, we observed that wavy fibers had a trend towards lower ADC ($11 \pm 0.49 \times 10^{-4}$ mm^2/s) values as compared to the mixed fibers ($11.3 \pm 0.11 \times 10^{-4}$ mm^2/s). ADC values in wavy fiber regions were significantly lower than in straight fiber regions ($12.3 \pm 0.48 \times 10^{-4}$ mm^2/s, $P = .006$, N = 3). Similarly, lower FA values were observed in wavy fiber regions (0.19 ± 0.02) compared to the mixed fiber regions (0.22 ± 0.03). FA values in wavy fiber regions were significantly lower than in dense fiber regions (0.215 ± 0.01, $P = .055$, N = 3) (Figure 5, *D*–*E*). Texture analysis masks of straight (red), mixed (green) and wavy (blue) Col1 fiber patterns are shown in Figure 5*F*.

Fibroblast Immunostaining

We performed immunostaining for activated fibroblasts to determine if infiltration of activated fibroblasts could explain the presence of higher Col1 fibers in necrotic regions. As shown in Figure 6, necrotic regions with dense Col1 fibers displayed strongly positive α-SMA stained activated fibroblasts.

Discussion

Col1 fibers appeared to mediate water diffusion and anisotropy as measured by diffusion MRI. In the tumor xenografts, hypoxic low Col1 fiber containing regions showed decreased ADC and FA values compared to normoxic regions that had significantly higher percent fiber volume. Necrotic high Col1 fiber containing regions showed increased ADC with decreased FA values compared to normoxic viable high Col1 fiber regions that had increased ADC with increased FA values. A good agreement of ADC and FA patterns was observed between *in vivo* and *ex vivo* images. Some tissue degradation may have occurred following tumor excision and fixation in PFA that may have reduced *ex vivo* FA values compared to *in vivo* FA values [29].

Ex vivo studies with human breast cancer tissue further validated our observations made with xenografts. Regions with high Col1 fiber content showed increased ADC and FA values, as evident from our fiber content quantification analysis. Within the constraints of our texture analysis approach, we found that a wavy fiber distribution had reduced ADC and FA values as compared to a fiber distribution containing mixed and straight fiber distribution. These data suggest that ADC and FA maps may provide non-invasive surrogate markers of Col1 fiber density.

Our finding that Col1 fiber density positively correlated with ADC values suggests that Col1 fibers enhance water diffusion in malignant breast cancers that are characterized by high Col1 fiber content [19]. In areas of dense Col1 fibers, we observed an increased FA as detected by DTI. This is in good agreement with two recent DTI studies of human articular cartilage [30], and porcine carotid artery [14], in which the directionality of water diffusion was consistent with the zonal distribution of Col1 fiber orientation. These results are also consistent with our previous study [20], where we observed regions with high Col1 fiber density had higher macro-molecular transport as compared to regions with lower Col1 fiber density. The dense aligned

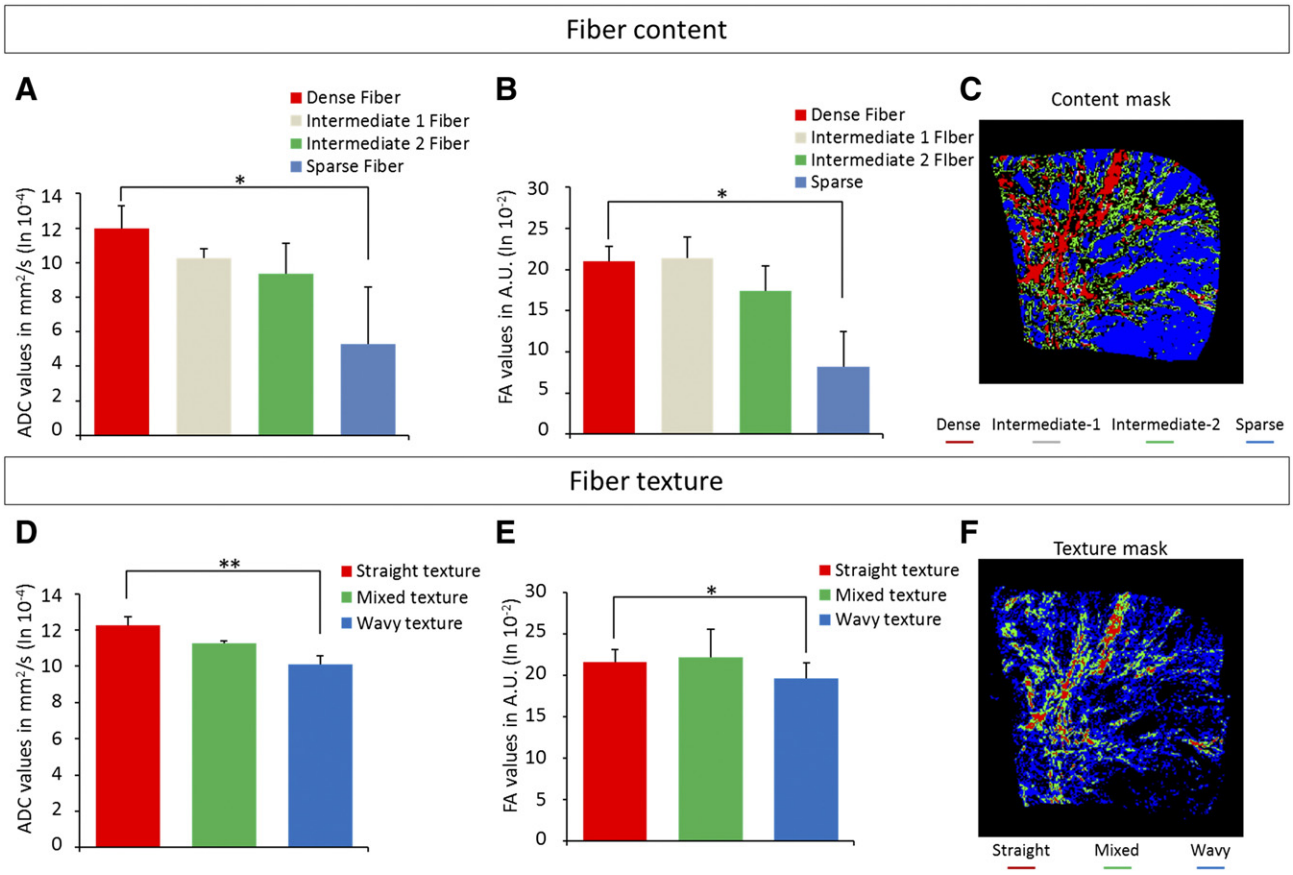

Figure 5. Quantification of DTI and Col1 data obtained from human breast cancer specimens. Significantly lower (A) ADC values and (B) FA values were observed in regions that contained sparse Col1 fibers compared to regions with dense Col1 fiber content (ADC: $P = .047$, FA: $P = .057$, N = 3). (C) Representative fiber content mask of dense (red), intermediate-1 (gray), intermediate-2 (green) and sparse fibers (blue). Significantly lower (D) ADC and (E) FA values were observed in the wavy texture pattern as compared to straight texture pattern regions (ADC: $P = .006$, FA: $P = .055$, N = 3). (F) Representative texture analysis mask of straight (red), mixed (green) and wavy fibers (blue). Values represent Mean ± SEM. $^{**}P \leq .01$, $^{*}P < .05$.

fibers observed in tumors may facilitate directional movement of molecules.

Recent human *in vivo* studies demonstrated that the ADC in breast cancers was significantly lower than that of benign breast lesions and normal breast tissue [31,32], and was accompanied by decreased FA in cancer *versus* normal tissue [32,33]. A decrease in the ADC and FA values observed in breast cancers could be due to the presence of hypoxia and the associated reduction of Col1 fibers [15]. Our findings also suggest that spatial maps of ADC and FA values of breast lesions may provide a more accurate characterization of cancer microenvironments [34].

The results obtained here strongly support investigating ADC and FA as noninvasive surrogates of Col1 fiber density. Our data are consistent with earlier studies demonstrating the facilitation of macromolecular transport by Col1 fibers [20]. The results obtained here suggest that low molecular weight agent transport through the

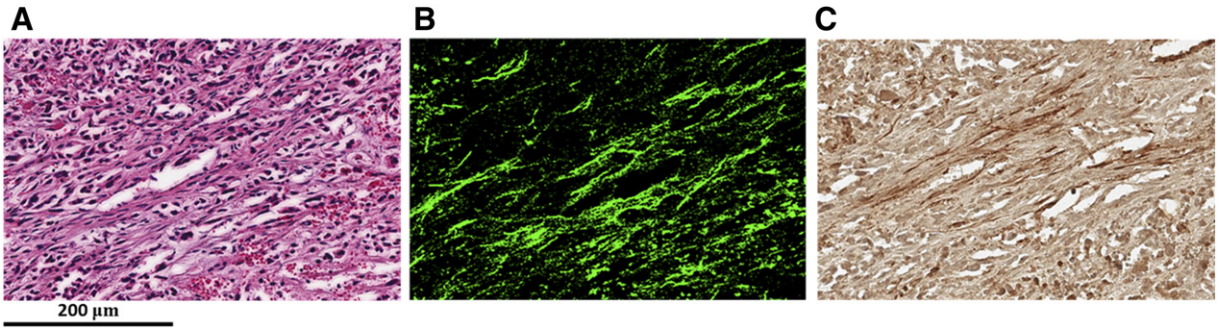

Figure 6. Immunohistochemistry staining of activated fibroblasts. Representative images from an (A) H&E section with (B) corresponding SHG image and (C) corresponding α-SMA staining. Scale bar of 200 μm for all images (A-C).

ECM is also mediated by Col1 fibers. Disorganized stroma in breast cancer biopsies has been associated with poor response to neoadjuvant chemotherapy [35]. Our data suggest that unorganized or sparsely distributed Col1 fibers may contribute to lower drug delivery.

ADC values increased but FA values decreased in necrotic regions compared to the normoxic viable regions, which could be due to the disorganized distribution of Col1 fibers in the necrotic regions. Since normoxic areas also contain higher Col1 fibers and are associated with higher ADC and FA, our data suggest that a combination of viable cells and high Col1 fiber content are required for water diffusion directionality. Increased Col1 fiber content within necrotic tumor regions may be an active process, or they may just be residual fibers left in these dead areas. The observation that the Col1 fiber volume was significantly higher in necrotic areas compared to normoxic viable areas, together with the presence of activated fibroblasts in these necrotic areas with high Col1 fiber density, suggests an active process mediated by the activated fibroblasts. The presence of increased Col1 fibers in necrotic tumor regions may also contribute to the increased ADC observed following cell death inducing treatments [36].

Noninvasive indices of Col1 fiber patterns using DTI may be used to assist in chemotherapy outcome prediction. Noninvasive DTI may be used as a surrogate marker to assess Col1 fiber density in breast cancers, as a marker of aggressiveness [2]. A decrease in ADC and FA values observed within a lesion could predict hypoxia and a pattern of high ADC with low FA values could predict necrosis. Our data support further validating the use of DTI parameters as surrogates for Col1 fiber patterns associated with specific tumor microenvironments.

Funding

This work was supported by National Institutes of Health R01 CA136576, R01 CA138515, R01 CA73850, R01 CA82337, R01 CA154725, R01 CA134695, P50 CA103175, and P30 CA006973.

Acknowledgements

We gratefully acknowledge expert assistance from Drs. Dmitri Artemov and Vadappuram Chacko. We thank Mr. Gary Cromwell for maintaining cells and inoculating tumors, and Ms. Flonne Wildes for monitoring xenograft growth.

References

[1] Brown E, McKee T, diTomaso E, Pluen A, Seed B, Boucher Y, and Jain RK (2003). Dynamic imaging of collagen and its modulation in tumors in vivo using second-harmonic generation. *Nat Med* **9**, 796–800.

[2] Provenzano PP, Inman DR, Eliceiri KW, Knittel JG, Yan L, Rueden CT, White JG, and Keely PJ (2008). Collagen density promotes mammary tumor initiation and progression. *BMC Med* **6**, 11.

[3] Sapudom J, Rubner S, Martin S, Kurth T, Riedel S, Mierke CT, and Pompe T (2015). The phenotype of cancer cell invasion controlled by fibril diameter and pore size of 3D collagen networks. *Biomaterials* **52**, 367–375.

[4] Burke KA, Dawes RP, Cheema MK, Van Hove A, Benoit DS, Perry SW, and Brown E (2015). Second-harmonic generation scattering directionality predicts tumor cell motility in collagen gels. *J Biomed Opt* **20**, 051024.

[5] Riching KM, Cox BL, Salick MR, Pehlke C, Riching AS, Ponik SM, Bass BR, Crone WC, Jiang Y, and Weaver AM, et al (2014). 3D collagen alignment limits protrusions to enhance breast cancer cell persistence. *Biophys J* **107**, 2546–2558.

[6] Cox TR and Erler JT (2011). Remodeling and homeostasis of the extracellular matrix: implications for fibrotic diseases and cancer. *Dis Model Mech* **4**, 165–178.

[7] Provenzano PP, Eliceiri KW, Campbell JM, Inman DR, White JG, and Keely PJ (2006). Collagen reorganization at the tumor-stromal interface facilitates local invasion. *BMC Med* **4**.

[8] Conklin MW, Eickhoff JC, Riching KM, Pehlke CA, Eliceiri KW, Provenzano PP, Friedl A, and Keely PJ (2011). Aligned Collagen Is a Prognostic Signature for Survival in Human Breast Carcinoma. *Am J Pathol* **178**, 1221–1232.

[9] Mohler W, Millard AC, and Campagnola PJ (2003). Second harmonic generation imaging of endogenous structural proteins. *Methods* **29**, 97–109.

[10] Mori S and Zhang JY (2006). Principles of diffusion tensor imaging and its applications to basic neuroscience research. *Neuron* **51**, 527–539.

[11] Budde MD, Janes L, Gold E, Turtzo LC, and Frank JA (2011). The contribution of gliosis to diffusion tensor anisotropy and tractography following traumatic brain injury: validation in the rat using Fourier analysis of stained tissue sections. *Brain J Neurol* **134**, 2248–2260.

[12] Basser PJ and Pierpaoli C (1996). Microstructural and physiological features of tissues elucidated by quantitative-diffusion-tensor MRI. *J Magn Reson B* **111**, 209–219.

[13] Concha L, Livy DJ, Beaulieu C, Wheatley BM, and Gross DW (2010). In vivo diffusion tensor imaging and histopathology of the fimbria-fornix in temporal lobe epilepsy. *J Neurosci* **30**, 996–1002.

[14] Ghazanfari S, Driessen-Mol A, Strijkers GJ, Kanters FM, Baaijens FP, and Bouten CV (2012). A comparative analysis of the collagen architecture in the carotid artery: second harmonic generation versus diffusion tensor imaging. *Biochem Biophys Res Commun* **426**, 54–58.

[15] Kakkad SM, Solaiyappan M, O'Rourke B, Stasinopoulos I, Ackerstaff E, Raman V, Bhujwalla ZM, and Glunde K (2010). Hypoxic Tumor Microenvironments Reduce Collagen I Fiber Density. *Neoplasia* **12**, 608–617.

[16] Krishnamachary B, Penet MF, Nimmagadda S, Mironchik Y, Raman V, Solaiyappan M, Semenza GL, Pomper MG, and Bhujwalla ZM (2012). Hypoxia Regulates CD44 and Its Variant Isoforms through HIF-1 alpha in Triple Negative Breast Cancer. *PLoS One* **7**.

[17] Aggarwal M, Mori S, Shimogori T, Blackshaw S, and Zhang J (2010). Three-dimensional diffusion tensor microimaging for anatomical characterization of the mouse brain. *Magn Reson Med* **64**, 249–261.

[18] Jiang HY, van Zijl PCM, Kim J, Pearlson GD, and Mori S (2006). DtiStudio: Resource program for diffusion tensor computation and fiber bundle tracking. *Comput Methods Programs Biomed* **81**, 106–116.

[19] Kakkad SM, Solaiyappan M, Argani P, Sukumar S, Jacobs LK, Leibfritz D, Bhujwalla ZM, and Glunde K (2012). Collagen I fiber density increases in lymph node positive breast cancers: pilot study. *J Biomed Opt* **17**, 116017 (1-7).

[20] Kakkad SM, Penet MF, Akhbardeh A, Pathak AP, Solaiyappan M, Raman V, Leibfritz D, Glunde K, and Bhujwalla ZM (2013). Hypoxic Tumor Environments Exhibit Disrupted Collagen I Fibers and Low Macromolecular Transport. *PLoS One* **8**, e81869.

[21] Egeblad M, Rasch MG, and Weaver VM (2010). Dynamic interplay between the collagen scaffold and tumor evolution. *Curr Opin Cell Biol* **22**, 697–706.

[22] Castellano G, Bonilha L, Li LM, and Cendes F (2004). Texture analysis of medical images. *Clin Radiol* **59**, 1061–1069.

[23] Haralick RM, Shanmuga K, and Dinstein I (1973). Textural Features for Image Classification. *IEEE Trans Syst Man Cybern* **Smc3**, 610–621.

[24] Dunn JC (1973). A Fuzzy Relative of the ISODATA Process and Its Use in Detecting Compact Well-Separated Clusters. *J Cybern* **3**, 32–57.

[25] Collignon A, Maes F, Delaere D, Vandermeulen D, Suetens P, and Marchal G (1995). Automated multi-modality image registration based on information theory. *Comp Imag Vis* **3**, 263–274.

[26] Dice LR (1945). Measures of the Amount of Ecologic Association between Species. *Ecology* **26**, 297–302.

[27] Miyamoto S, Ichihashi H, and Honda K (2008). Algorithms for Fuzzy Clustering Methods in c-Means Clustering with Applications Introduction. *Stud Fuzz Soft Comp* **229**, 9–42.

[28] Heo SC, Lee KO, Shin SH, Kwon YW, Kim YM, Lee CH, Kim YD, Lee MK, Yoon MS, and Kim JH (2011). Periostin mediates human adipose tissue-derived mesenchymal stem cell-stimulated tumor growth in a xenograft lung adenocarcinoma model. *Biochim Biophys Acta* **1813**, 2061–2070.

[29] Zhang JY, Jones MV, McMahon MT, Mori S, and Calabresi PA (2012). In vivo and ex vivo diffusion tensor imaging of cuprizone-induced demyelination in the mouse corpus callosum. *Magn Reson Med* **67**, 750–759.

[30] Deng X, Farley M, Nieminen MT, Gray M, and Burstein D (2007). Diffusion tensor imaging of native and degenerated human articular cartilage. *Magn Reson Imaging* **25**, 168–171.

[31] El Khouli RH, Jacobs MA, Mezban SD, Huang P, Kamel IR, Macura KJ, and Bluemke DA (2010). Diffusion-weighted Imaging Improves the Diagnostic Accuracy of Conventional 3.0-T Breast MR Imaging. *Radiology* **256**, 64–73.

[32] Partridge SC, Ziadloo A, Murthy R, White SW, Peacock S, Eby PR, DeMartini WB, and Lehman CD (2010). Diffusion tensor MRI: preliminary anisotropy measures and mapping of breast tumors. *J Magn Reson Imaging* **31**, 339–347.

[33] Baltzer PA, Schafer A, Dietzel M, Grassel D, Gajda M, Camara O, and Kaiser WA (2011). Diffusion tensor magnetic resonance imaging of the breast: a pilot study. *Eur Radiol* **21**, 1–10.

[34] Marusyk A, Almendro V, and Polyak K (2012). Intra-tumour heterogeneity: a looking glass for cancer? *Nat Rev Cancer* **12**, 323–334.

[35] Dekker TJA, Charehbili A, Smit VTHBM, ten Dijke P, Meershoek-Klein Kranenbarg E, van de Velde CJH, Nortier JWR, Tollenaar RAEM, Mesker WE, and Kroep JR (2015). Disorganised stroma determined on pre-treatment breast cancer biopsies is associated with poor response to neoadjuvant chemotherapy: Results from the NEOZOTAC trial. *Mol Oncol* **9**, 1120–1128.

[36] Weiss E, Ford JC, Olsen KM, Karki K, Saraiya S, Groves R, and Hugo GD (2016). Apparent diffusion coefficient (ADC) change on repeated diffusion-weighted magnetic resonance imaging during radiochemotherapy for non-small cell lung cancer: A pilot study. *Lung Cancer* **96**, 113–119.